

# X-ray Diffraction Broadening Analysis

---

**Popović, Stanko; Skoko, Željko**

*Source / Izvornik:* **Macedonian Journal of Chemistry and Chemical Engineering, 2015, 34, 39 - 49**

**Journal article, Published version**

**Rad u časopisu, Objavljena verzija rada (izdavačev PDF)**

<https://doi.org/10.20450/mjce.2015.642>

*Permanent link / Trajna poveznica:* <https://um.nsk.hr/um:nbn:hr:217:362836>

*Rights / Prava:* [Attribution-NonCommercial 4.0 International](#)/[Imenovanje-Nekomercijalno 4.0 međunarodna](#)

*Download date / Datum preuzimanja:* **2025-01-31**



*Repository / Repozitorij:*

[Repository of the Faculty of Science - University of Zagreb](#)



## X-RAY DIFFRACTION BROADENING ANALYSIS<sup>♦</sup>

Stanko Popović<sup>1,2\*</sup>, Željko Skoko<sup>2</sup>

<sup>1</sup>Croatian Academy of Sciences and Arts, Croatia

<sup>2</sup>Physics Department, Faculty of Science, University of Zagreb, Croatia

spopovic@phy.hr; zskoko@phy.hr

The microstructural parameters of a crystalline sample can be determined by a proper analysis of XRD line profile broadening. The observed XRD line profile,  $h(\varepsilon)$ , is the convolution of the instrumental profile,  $g(\varepsilon)$ , and pure diffraction profile,  $f(\varepsilon)$ , caused by small crystallite (coherent domain) sizes, by faultings in the sequence of the crystal lattice planes, and by the strains in the crystallites. Similarly,  $f(\varepsilon)$  is the convolution of the crystallite size/faulting profile,  $p(\varepsilon)$ , and the strain profile,  $s(\varepsilon)$ . The derivation of  $f(\varepsilon)$  can be performed from  $h(\varepsilon)$  and  $g(\varepsilon)$  by the Fourier transform method, which does not require mathematical assumptions. The analysis of  $f(\varepsilon)$  can be done by the Warren-Averbach method applied to the obtained Fourier coefficients. Simplified methods based on integral widths may also be used in studies where a good relative accuracy suffices. The relation among integral widths of  $f(\varepsilon)$ ,  $p(\varepsilon)$  and  $s(\varepsilon)$  can be obtained if one assumes bell-shaped functions for  $p(\varepsilon)$  and  $s(\varepsilon)$ . Integral width methods overestimate both strain and crystallite size parameters in comparison to the Warren-Averbach method. The crystallite size parameter is more dependent on the accuracy in the diffraction profile measurement, than it is the strain parameter. The precautions necessary for minimization of errors are suggested through examples. The crystallite size and strain parameters obtained by means of integral widths are compared with those which follow from the Warren-Averbach method. Recent approaches in derivation of microstructure are also mentioned in short.

**Keywords:** X-ray diffraction broadening; crystallite size and strain; deconvolution; integral width; Warren-Averbach method

### АНАЛИЗА НА ШИРОЧИНАТА НА РЕНДГЕНСКИТЕ ДИФРАКЦИОНИ МАКСИМУМИ

Микроструктурните параметри на кристален примерок можат да се определат со помош на соодветна анализа на проширувањето на профилите од рендгенската дифракција. Регистрираниот дифракционен профил,  $h(\varepsilon)$ , е конволуција на инструменталниот профил,  $g(\varepsilon)$ , и чистиот дифракционен профил,  $f(\varepsilon)$ , предизвикан од малите кристалитни димензии (кохерентен домен), потоа од несовершеностите во секвенциите од рамнините на кристалната решетка и од напрегањата во кристалитите. Слично,  $f(\varepsilon)$  е конволуција на кристалитниот големина/несовершенство профил,  $p(\varepsilon)$ , и профилот на напрегнатост,  $s(\varepsilon)$ . Одредувањето на  $f(\varepsilon)$  може да се изврши од  $h(\varepsilon)$  и  $g(\varepsilon)$  со помош на методот на Фуријеова трансформација, којашто не бара математички претпоставки. Анализата на  $f(\varepsilon)$  може да се изведе со помош на методот на Warren-Averbach применета на добиените Фуријеови коефициенти. Упростените методи засновани на интегралните широчини на профилите можат, исто така, да се користат и при студии каде што се достигнати релативно добри согласности. Зависноста помеѓу интегралните широчини на  $f(\varepsilon)$ ,  $p(\varepsilon)$  и  $s(\varepsilon)$  може да се добие ако се претпостават своновидни функции за  $p(\varepsilon)$  и  $s(\varepsilon)$ . Во споредба со методот на Warren-Averbach, методот на интегрална широчина ги преценува параметрите на напрегнатоста и на кристалитната големина. Параметарот на кристалитната големина е позависен од точноста на мерењето на дифракциониот профил во споредба со параметарот на напрегнатоста. Сугерирани се, низ примери, неопходните претпазливости за минимизирање на грешките. Параметрите на

<sup>♦</sup> Dedicated to Academician Gligor Jovanovski on the occasion of his 70<sup>th</sup> birthday.

кристалитната големина и на напрегнатоста добиени со помош на интегралната широчина се споредени со оние добиени со методот на Warren-Averbach. Накучо се наведени и неодамнешните сознанија во врска со определувањето на микроструктурата.

**Клучни зборови:** широчина на рендгенските дифракциони максимуми; кристалитна големина и напрегнатост; деконволуција; интегрална широчина; метода на Warren-Averbach

## 1. INTRODUCTION

Microstructural parameters of a given material, crystallite size, distribution of sizes, crystalline strain and stacking faults, can be determined by X-ray diffraction methods, in combination with other techniques, especially electron microscopy and diffraction. All information on microstructure is contained in its diffraction pattern and can be inferred by a proper decoding and interpretation of the pattern. As the crystallite size decreases below, say, 100 to 200 nm, and/or with the presence of strains, diffraction line profiles become measurably broader than the instrumental profile. The high angle diffraction lines are affected first, and the  $K\alpha_1\alpha_2$  spectral components eventually cease to be resolved. For the crystallite size of, say, 10 nm, high angle diffraction lines become very broad and diffuse and may disappear, depending also on the fraction of strains. Low angle diffraction lines also become broad. The derivation of microstructure depends strongly on the accuracy of the X-ray diffraction line profile measurement and on the minimization of errors inherent in the measurement, *e.g.* [1].

The crystallite size derived from diffraction pattern is a measure of the average thickness (in direction normal to diffracting crystal planes) of domains within which diffraction is coherent. This size does not necessarily correspond to the size of individual particles in a powder or grains in a polycrystal. Particles can be the single crystals, but each particle or grain may contain several diffracting domains. Therefore, it is very useful to combine X-ray diffraction with other techniques, such as transmission and scanning electron microscopy.

If a metal or a ductile material is deformed by cold work or other (thermal) treatment, its diffraction lines broaden, indicating that a disorder is introduced into the material. The nature of these changes may be [2]:

- the initial crystal grains are broken up into small crystallites (coherently diffracting domains) of the size up to, say, 100 to 200 nm;

- the crystallites remain large, say 1  $\mu\text{m}$  in size or bigger, but they are deformed, or suffer some kind of faultings, or undergo both effects;

- the material consists of small (even nanosized) crystallites, which are deformed and/or possess stacking faults, all these effects contributing to the broadening of diffraction lines.

The cold work produces arrays of dislocations, which have the effect to subdivide the grains into much smaller crystallites, which are also referred to as domains in literature. The domains may be mutually sufficiently disoriented that each domain diffracts incoherently with respect to other/neighbouring domains. The dislocations also produce tensile and compressive strains within the crystallites.

The first step before any attempt to analyze diffraction line broadening is to correct the *observed* (broadened) X-ray diffraction line profile of the studied sample for *instrumental* effects. A careful scan of a suitable standard sample, showing a negligible physical broadening will define the instrumental contribution to broadening. Details for standard specimen preparation are given in the literature, *e.g.* [3]. The most desirable approach in order to obtain the instrumental profiles is to anneal the sample showing broadened diffraction lines. Namely, the centroids of the *observed* profile of the studied sample,  $h(\varepsilon)$ , and of the *instrumental* profile,  $g(\varepsilon)$ , should be as close as possible. However, the annealed studied sample does not always give satisfactorily narrow diffraction lines; in that case the application of a suitable certified standard reference material is recommended. Detailed procedures for derivation of microstructural parameters are given in *e.g.* [4].

## 2. DECONVOLUTION

The *observed* X-ray diffraction line profile,  $h(\varepsilon)$ , is the convolution of the *instrumental* profile,  $g(\varepsilon)$ , and *pure diffraction* profile,  $f(\varepsilon)$  [5, 2]:

$$h(\varepsilon) = \int f(t)g(\varepsilon - t)dt \quad (1)$$

The variable  $\varepsilon$  measures the angular deviation of a point from the true Bragg angle  $2\theta_0$ ;  $\varepsilon$  and the auxiliary variable  $t$  have the dimension of  $2\theta$ .

Similarly to (1),  $f(\varepsilon)$  is the convolution of the *crystallite size/faulting* profile,  $p(\varepsilon)$ , and the *strain* profile,  $s(\varepsilon)$ :

$$f(\varepsilon) = \int p(t)s(\varepsilon - t)dt. \quad (2)$$

The derivation of  $f(\varepsilon)$  from (1) can be performed from the *measured*  $h(\varepsilon)$  and  $g(\varepsilon)$  by the Fourier transform method, usually cited as the Stokes method [6], where no assumption in the mathematical description of  $h(\varepsilon)$  and  $g(\varepsilon)$  is necessary [5]. A valuable feature of the Stokes method is that the broadening of the diffraction profiles due to the angular separation of the  $K\alpha_1\alpha_2$  spectral components is automatically allowed for.

The analysis of line broadening is based on the appropriate analysis of  $f(\varepsilon)$  in terms of *crystallite size/faulting* and *strain* parameters. Profile functions can be defined in the complex form as to be applicable to asymmetrical profiles:

$$\begin{aligned} h(\varepsilon) &= \sum_{t=-\varepsilon_M}^{+\varepsilon_M} H(t) \exp\left(-i\pi \frac{\varepsilon \cdot t}{\varepsilon_M}\right), \\ g(\varepsilon) &= \sum_{t=-\varepsilon_M}^{+\varepsilon_M} G(t) \exp\left(-i\pi \frac{\varepsilon \cdot t}{\varepsilon_M}\right), \\ f(\varepsilon) &= \sum_{t=-\varepsilon_M}^{+\varepsilon_M} F(t) \exp\left(-i\pi \frac{\varepsilon \cdot t}{\varepsilon_M}\right). \end{aligned}$$

The profiles are defined in the angular interval from  $2\theta_{-M}$  to  $2\theta_{+M}$   $[-\varepsilon_M, \varepsilon_M]$ . The interval should be chosen wide enough that beyond it the intensity of  $h(\varepsilon)$  and  $g(\varepsilon)$  can be considered to have fallen to the background level.

The Fourier coefficients of two measured profiles, of the studied sample,  $h(\varepsilon)$ , and of the standard sample,  $g(\varepsilon)$ , are given by summations:

$$\begin{aligned} H_{re}(t) &= h(0) + \sum_{\varepsilon=1}^{+\varepsilon_M} [h(\varepsilon) + h(-\varepsilon)] \cos\left(\pi \frac{\varepsilon \cdot t}{\varepsilon_M}\right), \\ H_{im}(t) &= \sum_{\varepsilon=1}^{+\varepsilon_M} [h(\varepsilon) - h(-\varepsilon)] \sin\left(\pi \frac{\varepsilon \cdot t}{\varepsilon_M}\right), \\ G_{re}(t) &= g(0) + \sum_{\varepsilon=1}^{+\varepsilon_M} [g(\varepsilon) + g(-\varepsilon)] \cos\left(\pi \frac{\varepsilon \cdot t}{\varepsilon_M}\right), \\ G_{im}(t) &= \sum_{\varepsilon=1}^{+\varepsilon_M} [g(\varepsilon) - g(-\varepsilon)] \sin\left(\pi \frac{\varepsilon \cdot t}{\varepsilon_M}\right). \end{aligned}$$

It follows from the Fourier integral theorem that the real and imaginary Fourier coefficients of pure physical diffraction profile  $f(\varepsilon)$  are given by equations:

$$F_{re}(t) = \frac{H_{re}(t)G_{re}(t) + H_{im}(t)G_{im}(t)}{G_{re}^2(t) + G_{im}^2(t)},$$

$$F_{im}(t) = \frac{H_{im}(t)G_{re}(t) - H_{re}(t)G_{im}(t)}{G_{re}^2(t) + G_{im}^2(t)}.$$

$$F(t) = [F_{re}^2(t) + F_{im}^2(t)]^{1/2}.$$

$H_{re}(t)$ ,  $H_{im}(t)$ ,  $G_{re}(t)$  and  $G_{im}(t)$  are the coefficients of  $h(\varepsilon)$  and  $g(\varepsilon)$ , respectively. The profile  $f(\varepsilon)$  can be synthesized as

$$f(\varepsilon) = F_{re}(0) + 2 \sum [F_{re}(t) \cos(\pi \varepsilon t / \varepsilon_M) + F_{im}(t) \sin(\pi \varepsilon t / \varepsilon_M)], \quad (3)$$

the summation being performed from  $t = 1$  to  $t'$ , and  $t'$  is that value of  $t$  for which

$$F_{re}(t > t') \text{ and } F_{im}(t > t')$$

have fallen practically to zero.

It is important to choose the adequate background level of the measured profile. There is a tendency to estimate the background level too high, due to overlapping of the adjacent diffraction lines and also due to the fact that for small crystallite size the tails of the diffraction line are rather long. The consequence is the so-called *hook effect* in the dependence of  $F(t)$  on  $t$ : the obtained value of  $F(0)$  is smaller than it should be. This can be avoided by choosing the background level of the studied sample to be equal to that of the annealed, standard, sample.

If the physical broadening is small compared to the instrumental broadening, the deconvolution may become rather unstable. If  $h(\varepsilon)$  is only, say, 20% broader than  $g(\varepsilon)$ , that gives an upper limit of about 100 to 200 nm for the determination of the crystallite size.

Experimental errors in the measurement of  $h(\varepsilon)$  and  $g(\varepsilon)$ , the finite angular interval in which the profiles are measured and the truncation of their tails may produce oscillations (*ripples*) of the derived ordinates of  $f(\varepsilon)$  at high values of  $\varepsilon$  in (3).

### 3. WARREN-AVERBACH METHOD

The analysis of  $f(\varepsilon)$  is usually performed by the Warren-Averbach method through the Fourier

coefficients obtained by deconvolution [5,6,7]. Namely, each coefficient is the product of the *crystallite size/faulting* parameter and the *strain* parameter, the latter depending on the order of diffraction maximum:

$$F(t) = F_{cf}(t) \cdot F_s(t, hkl). \quad (4)$$

That fact makes it possible to separate *crystallite size/faulting* parameter from the *strain* parameter for small (several initial) values of  $t$ , by using two or more diffraction orders for the same set of crystal lattice planes (eg.  $hkl$ ,  $2h\ 2k\ 2l$ ,  $3h\ 3k\ 3l$ ). The order  $t$  of the coefficients can be transformed into the order  $L$  according to the relation

$$L = \frac{\lambda \cdot t}{4(\sin \Theta_M - \sin \Theta_0)},$$

where  $L$  is the distance normal to the diffracting planes ( $hkl$ ), having the interplanar spacing  $d_{hkl}$ ,  $\lambda$  being the wavelength of X-rays. For small values of  $L$  the following approximation is valid:

$$\ln F(L, hkl) = \ln F_{cf}(L) - 2\pi^2 L^2 \langle e^2 \rangle_{WA} / (d_{hkl})^2 \quad (5)$$

The analysis, according to (4) and (5), provides in principle information on the (surface-weighted) crystallite size,  $\langle L \rangle_{WA}$ , distribution of sizes, deformation-twin faulting and the (averaged mean squared) strain over a distance  $L$  normal to diffracting crystal lattice planes. A series of plots of  $\ln F(L, hkl)$  versus  $1/(d_{hkl})^2$  are constructed for different values of  $L$ . For a given value of  $L$  the intercept on the ordinate axis gives the *size/faulting* coefficient,  $F_{cf}(L)$ , while the slope gives the mean squared strain,  $\langle e^2 \rangle_{WA}$ . The (negative) initial slope of the plot of  $F_{cf}(L)$  versus  $L$ , i.e., the first derivative of the plot at  $L = 0$ , is connected with the microstructural parameters:

$$-dF_{cf}(L)/dL = 1/\langle L \rangle_{WA} + 1/\langle L_f \rangle_{WA}. \quad (6)$$

$\langle L \rangle_{WA}$  is the crystallite size, as defined by the Warren-Averbach method, in the direction normal to the diffracting planes, whereas  $\langle L_f \rangle_{WA}$  is the contribution due to faultings on crystal lattice planes. In case that contribution due to faultings is small, the intercept of the initial slope of  $F_c(L)$  (subscript  $f$  omitted) versus  $L$  with the abscissa axis equals  $\langle L \rangle_{WA}$ . For a strain free sample, the analogous intercept on the abscissa axis of the plot  $F(L, hkl)$  versus  $L$  yields directly  $\langle L \rangle_{WA}$  in direction normal to the diffracting planes. The crystallite size distribution is given by the second derivative,  $d^2 F_c(L)/dL^2$ .

The second derivative cannot be negative, as the crystallite size distribution is positive. It follows that the plot of  $F_c(L)$  versus  $L$  should be concave upward, but never downward. If it happens that the plot is concave downward, i.e. the *hook effect* is present, this is an indication that the coefficient  $F(0)$  is smaller than it should be. Since  $F(0)$  is proportional to the area of the profile  $f(\varepsilon)$ , the reason for the *hook effect* may be the overestimation of the background level.

Contribution due to faultings in (6) may appear for a material which can be regarded structurally to be composed of well-defined layers. The faultings are random crystallographic misplacements of successive layers, i.e. random deviations from the correct sequence of layers (crystal lattice planes) according to requirements of the space group. The faultings may occur as a result of *cold work* (deformation fault) or *crystal growth* (twin fault). Not all diffraction lines are broadened or similarly broadened by the presence of faultings. A detailed description of the derivation of the faulting probability and the nature of faultings are given in e.g. [5].

#### 4. INTEGRAL WIDTH METHOD

On the other hand, simplified methods, which are based on the integral width,  $\beta_i$ , or full-width at half maximum,  $\beta_{1/2}$  (FWHM), of  $f(\varepsilon)$ , may be used in studies where a relative accuracy suffices. Simple procedures for derivation of the width  $\beta_i$  from the measured widths  $B_i$  and  $b_i$  of  $h(\varepsilon)$  and  $g(\varepsilon)$ , resp., can be found in e.g. [2]. These procedures are based on the following equation which can be derived from (1):

$$B_i = b_i \beta_i / \int g(\varepsilon) f(\varepsilon) d\varepsilon. \quad (7)$$

Similarly, the integral widths  $\beta_i$ ,  $\beta_{pi}$  and  $\beta_{si}$  of  $f(\varepsilon)$ ,  $p(\varepsilon)$  and  $s(\varepsilon)$ , resp., are connected by the equation

$$\beta_i = \beta_{pi} \beta_{si} / \int p(\varepsilon) s(\varepsilon) d\varepsilon. \quad (8)$$

In order to obtain the relation among the widths of  $h(\varepsilon)$ ,  $g(\varepsilon)$  and  $f(\varepsilon)$ , or among the widths of  $f(\varepsilon)$ ,  $p(\varepsilon)$  and  $s(\varepsilon)$ , one may assume bell-shaped functions for  $g(\varepsilon)$  and  $f(\varepsilon)$  in (7), or for  $p(\varepsilon)$  and  $s(\varepsilon)$  in (8). These assumptions, of course, affect the relations among the integral widths in question. The bell-shaped functions, usually used in the analysis of powder diffraction pattern, in the individual profile fitting, in the application of the

Rietveld refinement and in the crystal structure analysis, are:

- Cauchy (Lorentzian) function,  $C(\varepsilon) = (1 + K_C^2 \varepsilon^2)^{-1}$ , in literature used for  $p(\varepsilon)$  in case of a wide crystallite size distribution;
- modified Cauchy function,  $Q(\varepsilon) = (1 + K_Q^2 \varepsilon^2)^{-2}$ , used for  $s(\varepsilon)$ ;
- Gauss function,  $G(\varepsilon) = \exp(-K_G^2 \varepsilon^2)$ , used for  $s(\varepsilon)$ ;
- $S(\varepsilon) = \sin^2(K_S \varepsilon) / (K_S \varepsilon)^2$ , used for  $p(\varepsilon)$  in case of a narrow crystallite size distribution;
- Voigt function,  $V(\varepsilon)$ , used for both  $p(\varepsilon)$  and  $s(\varepsilon)$  [8];
- pseudo Voigt function,  $V_p(\varepsilon) = \eta C(\varepsilon) + (1 - \eta) G(\varepsilon)$ ,  $0 \leq \eta \leq 1$  [9].

The Voigt function, a convolution of the Cauchy and Gaussian functions, appears to be a better choice in description of both size and strain profiles [8, 10, 11]. The derived (volume-weighted) *crystallite size* parameter,  $L_{hkl}$ , and the (upper limit of) *strain* parameter,  $e_{hkl}$ , depend on assumptions for  $p(\varepsilon)$  and  $s(\varepsilon)$ , e.g. [12, 8, 13].

For instance, if  $p(\varepsilon)$  is described by the Cauchy function and  $s(\varepsilon)$  by the Gauss function, the following approximate relation, derived from (8), can be used [14, 15]:

$$\beta_i^2 = \beta_i \beta_{pi} + \beta_{si}^2. \quad (9)$$

By using the well-known Scherrer equation (in case the stacking faults broadening is negligible),  $\beta_{pi} = \lambda / (L_{hkl} \cos \Theta)$ , and the Wilson equation,  $\beta_{si} = 4e_{hkl} \tan \Theta$  (where  $e_{hkl} = \Delta d / \bar{d}$ ,  $\bar{d}$  is the average spacing and  $\Delta d$  its change due to the strain), it follows from (9):

$$\gamma^2 / \sin^2 \Theta = \lambda \gamma / (L_{hkl} \sin^2 \Theta) + (4e_{hkl})^2, \quad (10)$$

where  $\gamma = \beta_i \cdot \cos \Theta$ . All available diffraction orders from a given set of crystal lattice planes (or all diffraction maxima in case of a cubic sample) can be used to construct the linear plot  $\gamma^2 / \sin^2 \Theta$  against  $\gamma / \sin^2 \Theta$ . The size and strain parameters are found from the slope,  $\lambda / L_{hkl}$ , and the ordinate intercept,  $(4e_{hkl})^2$  [16, 13].

The shape of the crystallites may be assumed in case the integral width varies with the indices of diffraction lines. Let the mean shape of hexagonal crystallites be plate-like, which thick-

ness (in the direction of  $c$  axis) is much smaller than the base diameter (in the direction of  $a$  axis). In such a case, diffraction lines  $00l$  are much broader than the lines  $hk0$ , while the lines  $hkl$  are intermediate in broadening.

Both approaches, Warren-Averbach and integral width methods, depend, among others, on the estimated background level along the diffraction pattern and on the inevitable truncation of diffraction profile tails. The truncation-background level error distorts the Fourier coefficients of the diffraction profile and may contribute to the *hook effect* introducing errors in the size and strain parameter values ([5]). Instead of the theoretical value,  $\beta_i = I[-\infty, +\infty] / I(0)$ , the measured value is  $\beta_{iTB} = \beta_i [-\varepsilon_M, \varepsilon_M] - 2\varepsilon_M I(\varepsilon_M) / I(0)$ .  $\beta_{iTB}$  is the *truncated* integral width with the *background* below the profile subtracted (Fig. 1). In case  $-\varepsilon_M$  and  $\varepsilon_M$  are the points where the profile ordinates fall to the one hundredth of  $I(0)$  (this choice was arbitrary and corresponds to an average detection limit in intensity measurement), the following combined truncation-background level errors are obtained for the bell-shaped functions [17, 18]:

Function	$\beta_{iTB} / \beta_i$ for $I(\varepsilon_M) / I(0) = 0.01$
Cauchy	0.873
pseudo-Voigt	0.914
Voigt	0.915
Cauchy <sup>2</sup>	0.948
Gauss	0.973

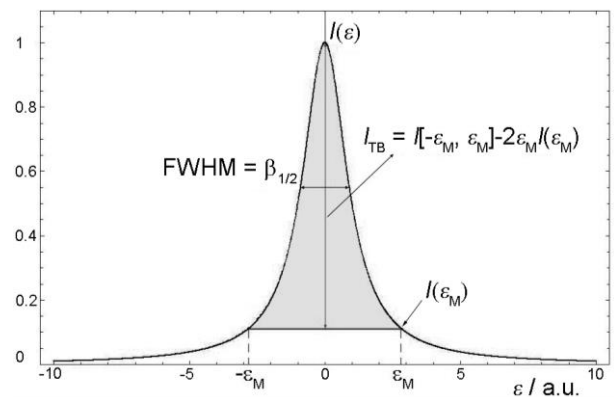


Fig. 1. A bell-shaped function with parameters used in the text.

It follows that the truncation-background level error more affects the functions, which are usually used in literature to describe the crystallite size parameter, than the ones used to describe the strain parameter, in line with the fact that the former have longer tails than the latter. The combined

error is the biggest for  $C(\varepsilon)$  (12.7 %), and the smallest for  $G(\varepsilon)$  (2.7 %). The error for  $V(\varepsilon)$  and  $V_p(\varepsilon)$  (8.5 %) is in between of those for  $C(\varepsilon)$  and  $G(\varepsilon)$ , as expected. This is in agreement with experimental evidence: the crystallite size is more affected by the accuracy with which the profile tails are measured than it is the strain.

## 5. EXAMPLES

Two cases of high symmetry, cubic, samples are presented: strain-free MgO showing only crystallite size broadening; NiO showing both crystallite size and strain broadening [17, 18]. In these cases, precautions for minimization of the combined truncation-background level error were undertaken. The influence of the background level error on the integral width, and consequently on the crystallite size and strain parameters, was found for a pure diffraction profile obtained by the Stokes method. Also, the broadening of diffraction lines which takes place during the phase transition  $\alpha\text{-In}_2\text{Se}_3 \leftrightarrow \beta\text{-In}_2\text{Se}_3$  is described briefly [19, 20]. The next example is the process of graphitization of the petroleum coke where all causes of broadening are present [21].

According to Warren [5], the background level of the broadened profile,  $h(\varepsilon)$ , should be equal to the level of the instrumental profile,  $g(\varepsilon)$ . This statement appears to be a very good approximation and was applied in the following examples. Diffractometers with adequate X-ray optics and narrow slits provide rather sharp profiles  $g(\varepsilon)$ , and their background level can be estimated with a satisfactory accuracy.

### 5.1. MgO

MgO ( $Fm\bar{3}m$ ,  $Z = 4$ ,  $a = 0.4213(1)$  nm at 25 °C) was prepared from basic magnesium carbonate by calcination from 600 to 1300 °C for 6 hours, followed by slow cooling inside the furnace to RT, in order to anneal strains. The widths of diffraction lines decreased as the calcination temperature increased. MgO<sub>1300</sub> showed very sharp diffraction lines, being practically as sharp as those of pure Ge (having micrometre sized grains) for which it was proved to represent the instrumental broadening. Therefore, line profiles of MgO<sub>1300</sub> were used as  $g(\varepsilon)$ 's in deconvolution of the line profiles of MgO<sub>600</sub> to MgO<sub>1000</sub> by the Stokes method. Five line profiles were analyzed, 200, 220, 222, 420 and 422. The Fourier coefficients obtained by deconvolution usually *irregularly oscillate* at higher

orders (Fig. 2). If all as-calculated Fourier coefficients, shown in Figure 2, were used in the synthesis of  $f(\varepsilon)$ , a *totally inadequate* result would be obtained.

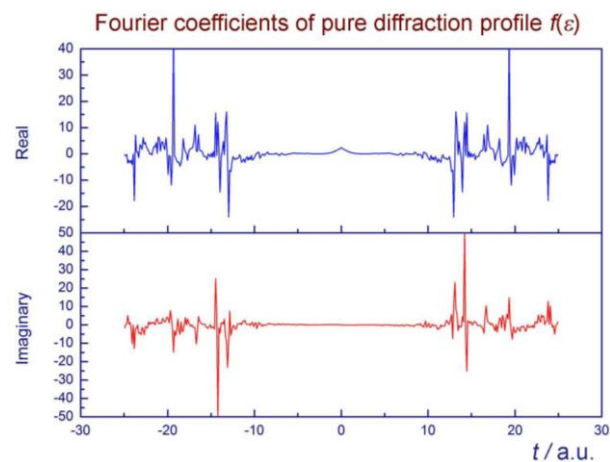


Fig. 2. As-calculated Fourier coefficients of pure diffraction profile,  $f(\varepsilon)$ , for 200 MgO<sub>650</sub>

Therefore, all as-calculated Fourier coefficients cannot be used either in the synthesis of a proper  $f(\varepsilon)$  or in the Warren-Averbach method. Instead, only low order as-calculated (say, first 20 to 40) coefficients, which gradually decreased as their order increased, were used. When they started to oscillate (say, above the 20<sup>th</sup> to 40<sup>th</sup> order), they were extrapolated asymptotically to zero as their order increased (Fig. 3). By using the coefficients selected in such a way, proper  $f(\varepsilon)$ 's were obtained, which could be nicely fitted by a Voigt function. The line profiles  $h(\varepsilon)$ ,  $g(\varepsilon)$  and  $f(\varepsilon)$  for the diffraction line 200 are shown in Figure 4 (dots: measured values for  $h(\varepsilon)$  and  $g(\varepsilon)$ , calculated values for  $f(\varepsilon)$ ; full lines: fitting by a Voigt function) and for the diffraction line 422 in Figure 5.

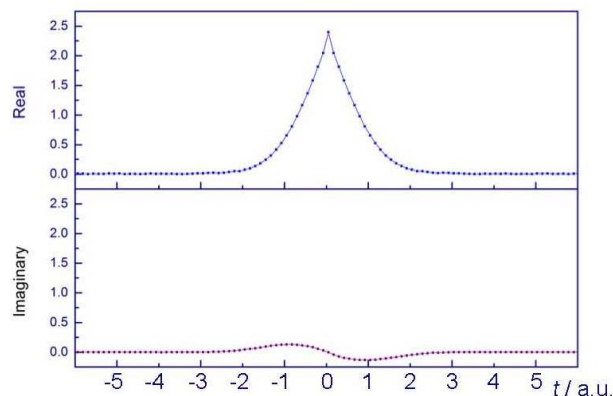
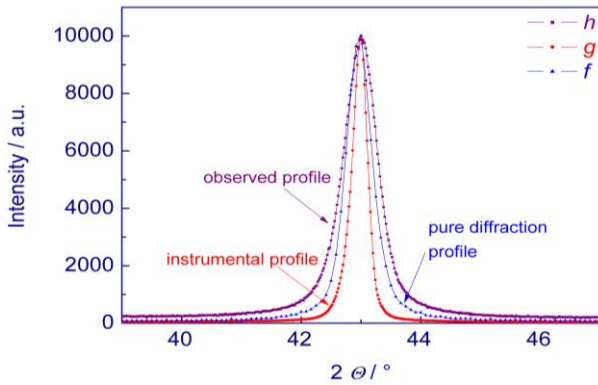
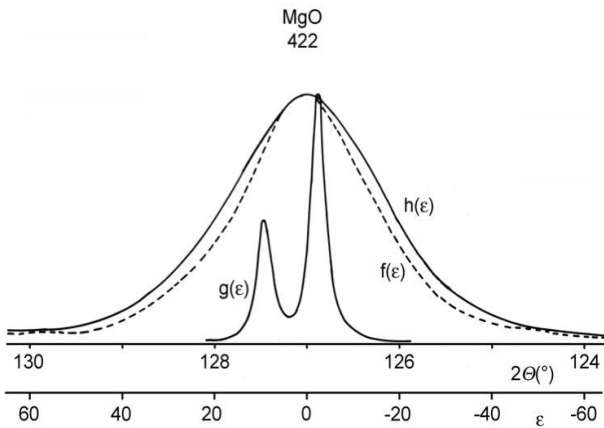


Fig. 3. Selected Fourier coefficients for 200 MgO<sub>650</sub> for synthesis of  $f(\varepsilon)$



**Fig. 4.** The line profiles 200 of MgO:  $h(\varepsilon)$  – MgO<sub>650</sub>,  $g(\varepsilon)$  – MgO<sub>1300</sub>, and  $f(\varepsilon)$  obtained by the Stokes method; dots: measured values for  $h(\varepsilon)$  and  $g(\varepsilon)$ , calculated values for  $f(\varepsilon)$ ; full lines: fitting by a Voigt function



**Fig. 5.** The line profiles 422 of MgO:  $h(\varepsilon)$  – MgO<sub>600</sub>,  $g(\varepsilon)$  – MgO<sub>1300</sub> and  $f(\varepsilon)$  obtained by the Stokes method

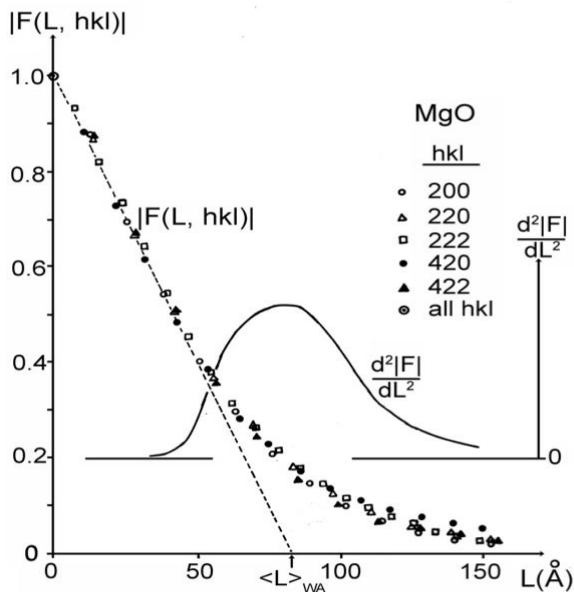


**Fig. 6.** Fourier coefficients  $F(L, hkl)$  vs  $L$  for five profiles of MgO<sub>600</sub> obtained by the Stokes method; crystallite size and crystallite size distribution derived by the Warren-Averbach method

The Fourier coefficients,  $F(L, hkl)$ , for the five line profiles vs  $L$  are shown in Figure 6. One can notice that all  $F(L, hkl)$ 's lie practically on the same curve. Therefore, it can be concluded that the small crystallite size was the only cause of diffraction broadening. Figure 6 also shows the value of the crystallite size,  $\langle L \rangle_{WA}$ , and the approximate crystallite size distribution,  $d^2F(L)/dL^2$ , derived by the method of Warren and Averbach. The *hook effect* was practically absent, which means that the background level was not overestimated. The described procedure is a proof that the Stokes method, if performed properly, yields  $f(\varepsilon)$ 's with minimum approximations.

Having calculated the Fourier coefficients of  $f(\varepsilon)$ 's,  $\beta_i$ 's were obtained by equation

$$\beta_i = F_{re}(0)(2\Theta_M - 2\Theta_{-M})/f(0), \quad (11)$$

$F_{re}(0)$  being the zero cosine Fourier coefficient. These  $\beta_i$ 's were used to calculate the crystallite size by using the Scherrer equation,  $L_{hkl} = \lambda/(\beta_i \cdot \cos \Theta)$ . The values of  $L_{hkl}$  were 15% bigger (as expected according to the literature, e.g. [13]), than  $\langle L \rangle_{WA}$ , but similar for various  $hkl$ . The values of  $\beta_i$ 's obtained by (11) were used to construct the plot according to equation (10) for MgO<sub>600</sub>, shown in Figure 7.

A straight line through the origin was obtained, this meaning that no strains were present in the sample. A crystallite size  $L_{hkl}$  of 10.0(5) nm was obtained from the slope of the straight line. As the calcination temperature of MgO increased from 600 to 1000 °C, the crystallite size increased from 10 to 44 nm, while the specific surface area decreased from 50 to 16 m<sup>2</sup>/g.

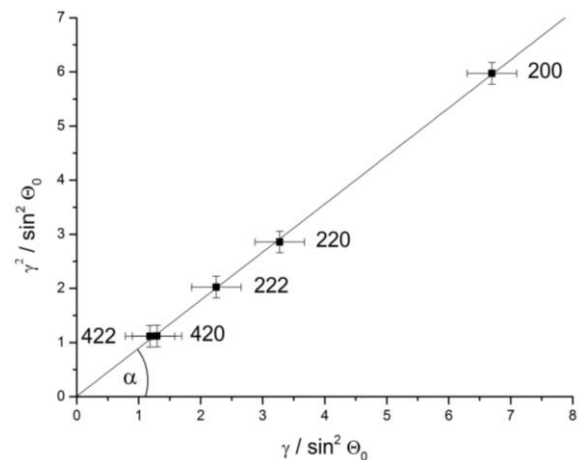


**Fig. 7.** The application of equation (10) on five profiles of MgO<sub>600</sub>;  $L_{hkl} = 10.0(5)$  nm; bars indicate estimated standard deviations



In order to find out the dependence of the integral width on the background level error for pure diffraction profile, obtained by the Stokes deconvolution, the background level was intentionally overestimated up to 5 %, in steps of 0.1 to 0.5 %. Of course, both the integral intensity of the profile (that is, the surface under the profile) and the intensity maximum of the profile decreased with the progressive overestimation of the background level. But, the decrease of the integral intensity was found bigger than the decrease of the maximum intensity. Therefore, the integral width decreased (for  $\approx 3\%$ ) with the overestimation of the background level (for 5%). The corresponding results for pure diffraction profile  $f(\varepsilon)$  of  $\text{MgO}_{650}$ , obtained by the Stokes method (Fig. 4), are shown in Figure 8. That dependence was fitted by a third order polynomial function. The extrapolation of that dependence to the point of zero background level overestimation may yield a true background level of diffraction profile; this procedure thus eliminates a possible initial error in the background level. The corresponding dependence of the crystallite size on the background overestimation is shown in Figure 9 [17, 18].

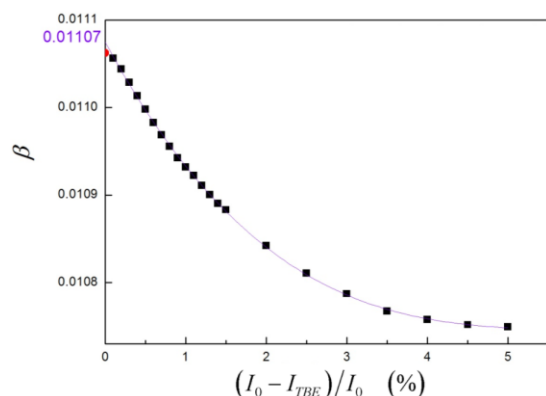


**Fig. 8.** Dependence of the integral width of pure diffraction profile  $f(\varepsilon)$  of  $\text{MgO}_{650}$ , obtained by the Stokes method (Fig. 4.), on the relative overestimation of the background level

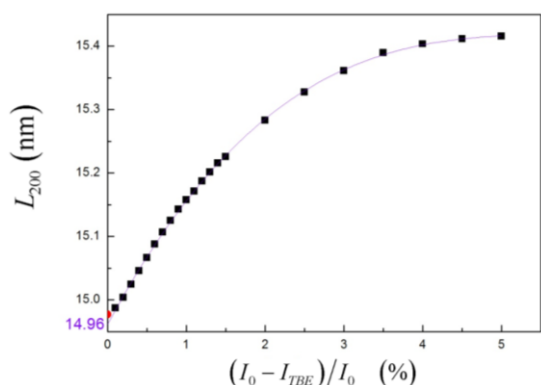


**Fig. 9.** Dependence of the crystallite size of  $\text{MgO}_{650}$  (Figs. 4, 8) on the relative overestimation of the background level

## 5.2. NiO

NiO ( $Fm\bar{3}m$ ,  $Z = 4$ ,  $a = 0.4177(1)$  nm at 25 °C) obtained from  $\text{Ni}(\text{OH})_2$  by thermal decomposition showed rather broad diffraction lines. Diffraction lines of Ge powder, intimately mixed with NiO, were used as  $g(\varepsilon)$ 's. As  $\beta$ 's of NiO, deduced by the Stokes method (following the procedure described above for  $\text{MgO}$ ), did not vary with  $\Theta$  either as  $1/\cos\Theta$  or  $\tan\Theta$ , it was concluded that both small crystallite size and strain caused broadening. The application of equation (10) on three diffraction line profiles is shown in Figure 10. It may be proposed that the hexagonal plates of  $\text{Ni}(\text{OH})_2$  split into layers of NiO by the thermal treatment at moderate temperatures; more details are given in [22].

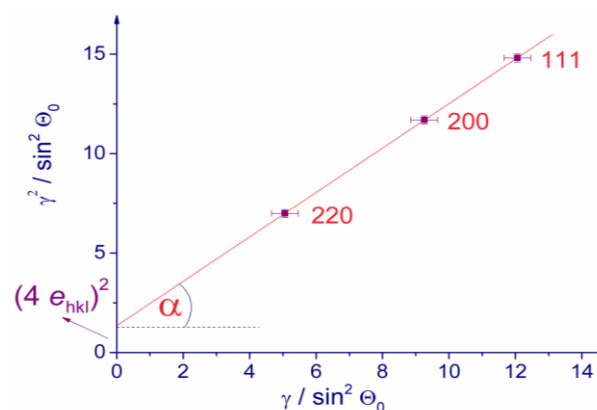


**Fig. 10.** The application of equation (10) on three profiles of NiO;  $L_{hkl} = 8.3(5)$  nm,  $e_{hkl} = 6.0(5) \times 10^{-3}$ ; bars indicate estimated standard deviations

## 5.3. Phase transition $\alpha\text{-In}_2\text{Se}_3 \leftrightarrow \beta\text{-In}_2\text{Se}_3$

$\text{In}_2\text{Se}_3$  exhibits at least four polytypic phase transitions in the interval from low temperature to the melting point [19, 20]. The transition  $\alpha\text{-In}_2\text{Se}_3 \leftrightarrow \beta\text{-In}_2\text{Se}_3$  as detected by X-ray diffraction is shown in Figure 11. Crystal data for these two phases are:

$$\alpha\text{-In}_2\text{Se}_3: R\bar{3}m, Z = 3, a = 0.4025(5), \\ c = 2.8762(7) \text{ nm at } 25 \text{ }^\circ\text{C},$$

$$\beta\text{-In}_2\text{Se}_3: R\bar{3}m, Z = 3, a = 0.4000(8), \\ c = 2.833(1) \text{ nm at } 205 \text{ }^\circ\text{C}.$$

One can notice the shift of diffraction lines with the change of temperature due to thermal expansion. It is similar for both  $\alpha$  and  $\beta$  phases:  $19/(10^6 \text{ }^\circ\text{C})$  along the  $c$  axis and  $3/(10^6 \text{ }^\circ\text{C})$  along the  $a$  axis. A big temperature hysteresis is present:

the transition  $\alpha\text{-In}_2\text{Se}_3 \rightarrow \beta\text{-In}_2\text{Se}_3$  takes place above 200 °C, while the reversal transition,  $\beta\text{-In}_2\text{Se}_3 \rightarrow \alpha\text{-In}_2\text{Se}_3$ , below 80 °C. These temperatures depend on the synthesis and previous history of the sample. For a polycrystalline sample, having highly oriented grains, the transition  $\beta\text{-In}_2\text{Se}_3 \rightarrow \alpha\text{-In}_2\text{Se}_3$  may take place between 80 and 50 °C, while a powdered sample can be undercooled and be stable in the  $\beta$ -phase below the room temperature. The broadening of diffraction lines is pronounced during the phase transitions indicating an increased disorder inside crystallites. The separation of the spectral doublet  $\text{CuK}\alpha_{1,2}$  is hardly visible during the transitions. That separation is increased a little at temperatures before and after phase transitions.

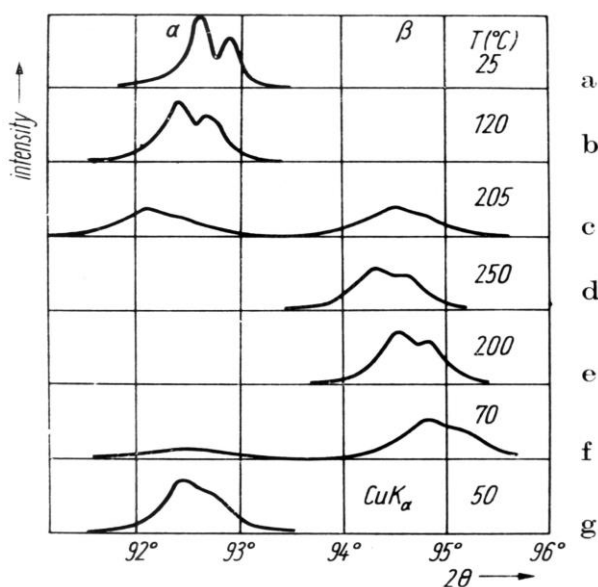


**Fig. 11.** Diffraction line 0 0 27 of  $\text{In}_2\text{Se}_3$  at different temperatures, exhibiting broadening during the phase transition  $\alpha\text{-In}_2\text{Se}_3 \leftrightarrow \beta\text{-In}_2\text{Se}_3$

#### 5.4. Graphitization of petroleum coke

This process represents a gradual transition from the petroleum coke toward the non-graphitic carbon, the graphitic carbon and the crystalline graphite ( $P6_3/mmc$ ,  $Z = 4$ ,  $a = 0.2460(1)$ ,  $c = 0.6708(2)$  nm at 25 °C) during a gradual increase of temperature. Petroleum coke consists of minute grains in which there are several (say, ten) roughly parallel layers, having a diameter of 3 to 4 nm, which are mutually randomly oriented about the layer normal. X-ray diffraction pattern is typical for a random layer structure [5], showing symmetrical broad lines 002 and 004 and asymmetrical 2D bands 10 and 11 (Figs. 12a, 12b). As the temperature increases, the 2D bands sharpen and move

toward smaller Bragg angles, but retain their asymmetrical shape. This indicates an increase of the layer diameter; however, the layers remain in random mutual orientation. The lines 002 and 004 also sharpen with temperature and shift toward higher Bragg angles, indicating a decrease of strains and an increase of number of layers in grains. Above 1600 °C a very broad line 006 also appears in diffraction pattern. After heating to 1500 °C and to 2150 °C the average interlayer spacing decreases to 0.3440 nm and to 0.3425 nm, resp., as measured at room temperature.

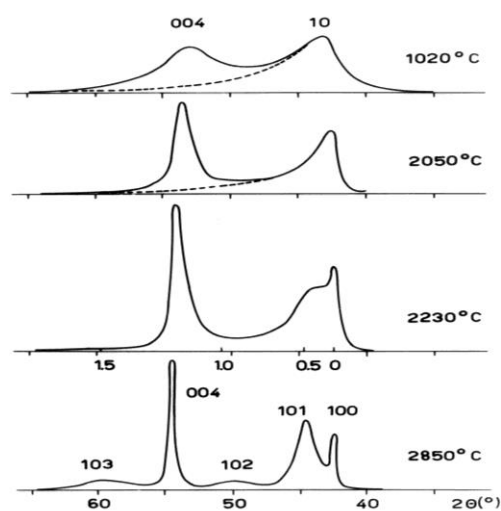


**Fig. 12a.** Parts of X-ray diffraction patterns of nongraphitic and graphitic carbons heated at high temperatures (patterns taken at room temperature after cooling)

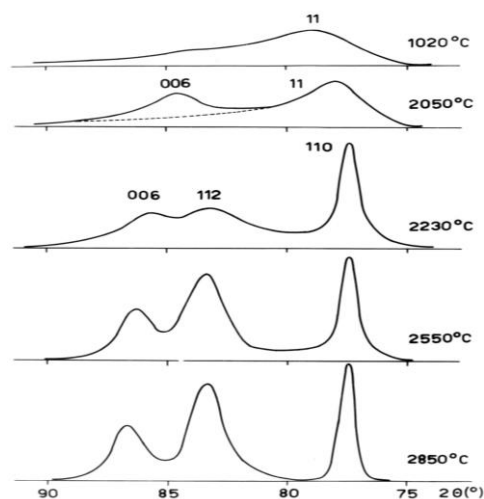


**Fig. 12b.** Parts of X-ray diffraction patterns of nongraphitic and graphitic carbons heated at high temperatures (patterns taken at room temperature after cooling)

Diffraction patterns of samples heated up to 2200 °C are typical for the non-graphitic carbon. But the pattern of the sample heated at 2230 °C

shows a beginning of splitting of 2D bands into 3D lines: 10 into 100, 101 and 102, and 11 into 110 and 112 (Figs. 12a, 12b). These modulations indicate the start of graphitization. The neighbouring layers, having reached the diameter of  $\sim 10$  nm, begin to undergo mutual graphitic ordering. Also, diffraction lines 00 $l$  shift abruptly toward higher Bragg angles, indicating an abrupt decrease of the interlayer spacing (Fig. 13). As the temperature increases further, up to 3000 °C, all diffraction lines sharpen, due to an increase of the crystallite size and their further ordering (a decrease of strains), approaching the structure of highly crystalline graphite (Fig. 14). The interlayer spacing gradually approaches the value typical for graphite. The fraction of layers involved in faultings falls from 1 to 0.15 upon heating from room temperature to 3000 °C [21].

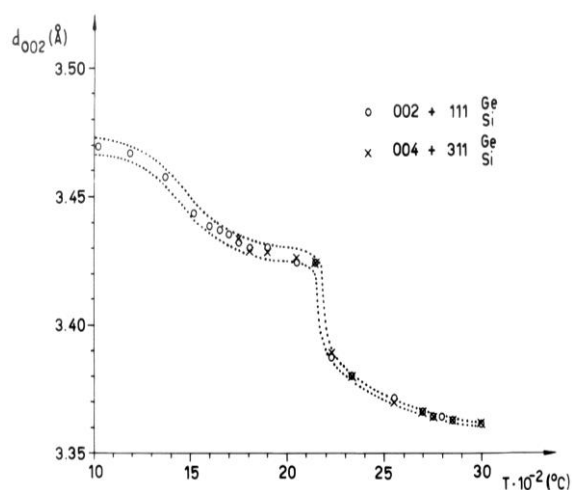


**Fig. 13.** The interlayer spacing,  $d_{002}$ , of nongraphitic and graphitic carbons heated at high temperatures (measured at room temperature after cooling)

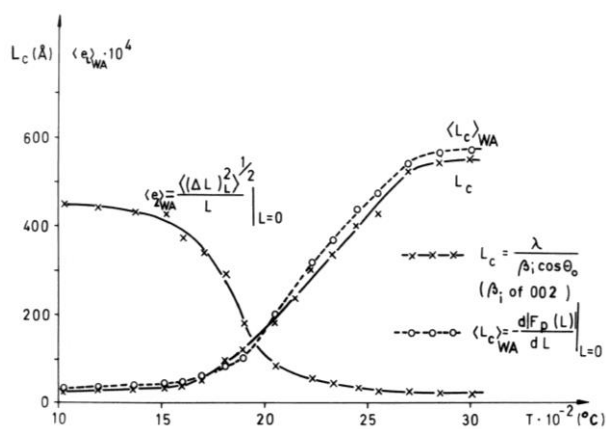


**Fig. 14.** The crystallite size (in direction normal to the graphite layers) determined by the methods of Warren and Averbach,  $\langle L_c \rangle_{WA}$ , and Scherrer,  $L_c$ , and the lattice strain,  $\langle (e^2)_{WA} \rangle^{1/2}$ , of nongraphitic and graphitic carbons heated at high temperatures (all measured at room temperature after cooling)

## 6. OTHER APPROACHES

The described methods for interpretation of diffraction broadening have been developed before the introduction of sophisticated instrumentation and fast computers. Nowadays, reliable diffraction data can be collected by a modern diffractometer and the deconvolution can be performed in a very short time. For instance, the Stokes deconvolution followed by the Warren-Averbach and integral widths analyses has been implemented in easy-to-use program, *XBroad*, for a quick determination of the basic microstructural information from X-ray powder diffraction patterns [23].

The introduction of *analytical functions* to fit diffraction line profiles has been a great advancement in interpretation of diffraction patterns. That has led to the development of the *Rietveld method* [24], to diffraction pattern decomposition techniques [25] and to the general concept of the *whole powder pattern fitting* (WPPF), *e.g.* [26].

The *whole powder pattern modelling* (WPPM) allows a simultaneous processing of the whole X-ray diffraction pattern; it is based on a suitable model of domain size/shape and strain, without using arbitrary analytical profile functions, *e.g.* [27]. These new approaches have been proved to be very useful.

The known crystal structure of a given substance can be refined, *e.g.*, as a function of temperature or pressure, using the Rietveld method. That method is a so-called *full pattern analysis technique*. A model of the crystal structure, together with instrumental and microstructural information, are used to generate the theoretical diffraction pattern that can be compared to the observed pattern. The least squares procedure is then used to minimize the difference between the calculated pattern and the observed pattern by adjusting model parameters. That procedure may result in determination of the crystal structure and microstructural parameters; however, it is rather challenging due to the overlap of diffraction lines in the X-ray powder diffraction pattern.

## REFERENCES

- [1] R. Delhez, Th. de Keijser, E. J. Mittemeijer, Accuracy of crystallite size and strain values from X-ray diffraction line profiles using Fourier series; In: *Accuracy in Powder Diffraction*, NBS Special Publication No. 567, S. Block, C. R. Hubbard (Eds), Washington DC, National Bureau of Standards, 1980, pp. 213–253.
- [2] H. P. Klug, L. E. Alexander, *X-ray Diffraction Procedures*, New York, John Wiley, 1974.
- [3] J. G. M. van Berkum, G. J. M. Sprong, Th. de Keijser, R. Delhez, E. J. Sonneveld, The optimum standard spec-

- imen for X-ray diffraction line-profile analysis, *Powder Diffraction* **10**, 129–139 (1995).
- [4] D. Balzar, N. Audebrand, M. Daymond, A. Fitch, A. Hewat, J. I. Langford, A. Le Bail, D. Louër, O. Masson, C. N. McCowan, N. C. Popa, P. W. Stephens, B. Toby, Size-strain line-broadening analysis of the ceria round-robin sample, *J. Appl. Cryst.* **37**, 911–924 (2004).
- [5] B. E. Warren, *X-ray Diffraction*, Reading, MS, Addison-Wesley, 1969 / Dover, NY, Mineola, 1990.
- [6] A. R. Stokes, A numerical Fourier-analysis method for the correction of widths and shapes of lines on X-ray powder photographs, *Proc. Phys. Soc. London*, **61**, 382–391 (1948).
- [7] B. E. Warren, B. L. Averbach, The effect of cold-work distortion on X-ray patterns, *J. Appl. Phys.* **21**, 595–599 (1950).
- [8] J. I. Langford, A rapid method for analysing the breadths of diffraction and spectral lines using the Voigt function, *J. Appl. Cryst.* **11**, 10–14 (1978).
- [9] P. Thompson, D. E. Cox, J. B. Hastings, Rietveld refinement of Debye-Scherrer synchrotron X-ray data from  $\text{Al}_2\text{O}_3$ , *J. Appl. Cryst.* **20**, 79–83 (1987).
- [10] J. I. Langford, Diffraction line broadening analysis; In: *Accuracy in Powder Diffraction*, NBS Special Publication No. 567, S. Block, C. R. Hubbard (Eds), Washington DC, National Bureau of Standards, 1980, pp. 255–269.
- [11] J. I. Langford, Use of pattern decomposition or simulation to study microstructure: theoretical considerations; In: *IUCr Monographs on Crystallography, Defect and Microstructure Analysis by Diffraction*, R. L. Snyder, J. Fiala, H. J. Bunge, (Eds), Oxford, Oxford University Press, 1999, pp. 59–81.
- [12] W. Ruland, The separation of line broadening effects by means of line-width relations, *J. Appl. Cryst.* **1**, 90–101 (1968).
- [13] D. Balzar, S. Popović, Reliability of the simplified integral-breadth methods in diffraction line-broadening analysis, *J. Appl. Cryst.* **29**, 16–23 (1996).
- [14] F. R. L. Schoening, Strain and particle size values from X-ray line breadths, *Acta Cryst.* **18**, 975–976 (1965).
- [15] N. C. Halder, C. N. J. Wagner, Separation of particle size and lattice strain in integral breadth measurements, *Acta Cryst.* **20**, 312–313 (1966).
- [16] S. Popović, Application of bell-shaped functions in X-ray diffraction broadening analysis, *Croat. Chem. Acta* **57**, 749–755 (1984).
- [17] S. Popović, Ž. Skoko, G. Štefanić, Factors affecting diffraction broadening analysis, *Z. Kristallogr. Proc.* **1**, 55–62 (2011).
- [18] Ž. Skoko, S. Popović, G. Štefanić, Dependence of microstructure on errors in X-ray diffraction profile measurement, *J. Mater. Sci. Eng.* **A3**, 690–697 (2013).
- [19] S. Popović, B. Čelustka, D. Bidjin, X-ray diffraction measurement of lattice parameters of  $\text{In}_2\text{Se}_3$ , *Phys. Stat. Sol. A* **6**, 301–304 (1971).
- [20] S. Popović, A. Tonejc, B. Gržeta, B. Čelustka, R. Trojko, Revised and new crystal data for indium selenides, *J. Appl. Cryst.* **12**, 416–420 (1979).
- [21] S. Popović, Analysis of X-ray diffraction line broadening, *Izvj. Jugoslav. centr. krist.*, Yugoslav (Croatian) Academy of Sciences and Arts **12**, 47–80 (1977).
- [22] C. L. Cronan, F. J. Micale, M. Topić, H. Leidheiser Jr., A. C. Zettlemoyer, S. Popović, Surface properties of  $\text{Ni}(\text{OH})_2$  and  $\text{NiO}$ , *J. Colloid Interface Sci.* **55**, 546–557 (1976).
- [23] Ž. Skoko, J. Popović, K. Dekanić, V. Kolbas, S. Popović, XBroad-program for extracting basic microstructure information from XRD pattern in few clicks, *J. Appl. Cryst.* **45**, 594–597 (2012).
- [24] R. A. Young, *The Rietveld Method*. Oxford, Oxford University Press, 1993.
- [25] J. I. Langford, D. Louër, Powder diffraction, *Rep. Prog. Phys.* **59**, 131–234 (1996).
- [26] P. Scardi, A new whole-powder pattern-fitting approach; In: *IUCr Monographs on Crystallography, Defect and Microstructure Analysis by Diffraction*, R. L. Snyder, J. Fiala, H. J. Bunge (Eds), Oxford, Oxford University Press, 1999, pp. 570–596.
- [27] P. Scardy, M. Leoni, Y. H. Dong, Whole powder pattern modelling, *IUCr Commission on Powder Diffraction, Newsletter*, **24**, 23–24 (2000).

